Hearing Research 390 (2020) 107928

Contents lists available at ScienceDirect

Hearing Research

journal homepage: www.elsevier.com/locate/heares

Research Paper

# Simultaneous rather than retrograde spiral ganglion cell degeneration following ototoxically induced hair cell loss in the guinea pig cochlea

Dyan Ramekers [a, b], Sjaak F.L. Klis [a, b], Huib Versnel [a, b, *]

[a] Department of Otorhinolaryngology and Head & Neck Surgery, University Medical Center Utrecht, Utrecht University, Room G.02.531, P.O. Box 85500, 3508 GA, Utrecht, the Netherlands
[b] UMC Utrecht Brain Center, Utrecht University, the Netherlands

ARTICLE INFO

*Article history:*
Received 20 February 2019
Received in revised form
12 February 2020
Accepted 17 February 2020
Available online 24 February 2020

*Keywords:*
Auditory nerve
Hearing loss
Neurodegeneration
eCAP
Cochlear implant
Guinea pig

ABSTRACT

Severe damage to the organ of Corti leads to degeneration of the spiral ganglion cells (SGCs) which form the auditory nerve. This degeneration starts at the level of synaptic connection of the peripheral processes (PPs) of SGCs with the cochlear hair cells. It is generally thought that from this point SGC degeneration progresses in a retrograde fashion: PPs degenerate first, followed by the SGC soma with a delay of several weeks to many months. Evidence for this course of events, both in animals and in humans, is not unambiguous, while this knowledge is important since the presence or absence of the different neural elements may greatly influence the response to electrical stimulation with a cochlear implant (CI). We therefore aimed to provide a comprehensive account of the course of SGC degeneration in the guinea pig cochlea after ototoxic treatment. Histological analysis of eighteen healthy and thirty-three deafened cochleas showed that the degeneration of SGCs and their peripheral processes was simultaneous rather than sequential. As the site of excitation for electrical stimulation with a CI may depend on the course of degeneration of the various neural elements, this finding is relevant both for understanding the electrophysiological mechanisms behind cochlear implantation and for recent efforts to induce PP resprouting for improved electrode-neural interface. Since excitation of the PPs is often thought to result in (secondary) longer-latency activity, we tested the hypothesis that having relatively many PPs produces a larger $N_2$ peak in the electrically evoked compound action potential (eCAP); the present findings however do not support this theory. The course of the degeneration process may vary among species, and may depend on the cause of deafness, but the present findings at least indicate that gradual retrograde degeneration of the auditory nerve is not an elemental process following severe damage to the organ of Corti.



## 1. Introduction

Severe trauma to the organ of Corti, including loss of inner hair cells and supporting cells, leads to progressive loss of spiral ganglion cells (SGCs; Ylikoski et al., 1974; Spoendlin, 1975; Webster and Webster, 1981; Versnel et al., 2007; Zilberstein et al., 2012). The rate of this degeneration varies among species and with type and severity of the trauma (Spoendlin, 1975). In several studies the degeneration is characterized as being retrograde, affecting the peripheral processes (PPs) before the SGC somata (Spoendlin, 1975, 1984 [humans, cats, guinea pigs]; Leake and Hradek, 1988 [cats]; Shepherd and Javel, 1997 [cats]). Spoendlin (1975) identified damage to the unmyelinated portion of the PP as the initiation for retrograde degeneration in cats, after which it takes weeks for its myelinated part to degenerate, followed by the entire SGC within months. Similar reports followed from studies in humans (Otte et al., 1978; Hinojosa and Marion, 1983; Nadol, 1990) and in cats (Liberman and Kiang, 1978). Conversely, there have also been reports of simultaneous rather than sequential retrograde degeneration in humans (Hinojosa and Marion, 1983; Nadol et al., 1989; Spoendlin and Schrott, 1989), in cats (Spoendlin, 1984) and in

*Abbreviations:* ABR, auditory brainstem response; CI, cochlear implant; eCAP, electrically evoked compound action potential; OSL, osseous spiral lamina; PP, peripheral process; SNHL, sensorineural hearing loss; SGC, spiral ganglion cell

* Corresponding author. Department of Otorhinolaryngology and Head & Neck Surgery, University Medical Center Utrecht, Utrecht University, Room G.02.531, P.O. Box 85500, 3508 GA, Utrecht, the Netherlands.
*E-mail addresses:* d.ramekers@umcutrecht.nl (D. Ramekers), s.klis@umcutrecht.nl (S.F.L. Klis), h.versnel@umcutrecht.nl (H. Versnel).

https://doi.org/10.1016/j.heares.2020.107928

guinea pigs (Wise et al., 2005).

This course of degeneration is relevant for cochlear implantation since the various neural elements respond differently to electrical stimulation. An auditory nerve consisting predominantly of monopolar cells (i.e., cells without PPs) that are separated from the electrode array by the bony modiolar wall arguably responds differently to electrical stimulation than a nerve with healthy PPs protruding radially through the bony boundaries towards the electrode array. In addition, this course of degeneration is relevant with respect to recent therapeutical strategies aimed at regrowing PPs towards the CI electrode (e.g., Senn et al., 2017). Either – in case of retrograde degeneration – it is crucial to identify the time frame within which there exists a monopolar cell (in between PP degeneration and subsequent SGC soma loss), or, in case of simultaneous degeneration, the actual benefit of PP-regrowing strategies may become disputable.

Both human and animal studies reporting on the course of degeneration mainly involve case reports without accurate quantification. Our main goal was therefore to provide a detailed characterization of the course of SGC degeneration, by means of histological quantification of SGCs and their PPs in the ototoxically deafened guinea pig cochlea.

By determining the packing densities of SGC somata and the myelinated portion of their PPs between normal-hearing guinea pigs and guinea pigs 1, 2, 6, and 14 weeks after deafening, a detailed time course of the degeneration process of these neural elements is presented. In addition, the functional contribution of the surviving elements was assessed using the electrically evoked compound action potential (eCAP). Since the absolute eCAP amplitude is not a reliable measure of neural survival (Ramekers et al., 2014, 2015a), we here focused on the ratio of the two negative peaks in the eCAP. On the one hand this comparison can be informative of the electrophysiological condition of the degenerating SGC population; on the other hand, comparing this ratio to the ratio of PP and SGC packing densities may clarify which neural elements are essential for excitation by electrical stimulation from cochlear implants. The present electrophysiological data therefore provide unique additional information to the detailed histological analysis of the SGC soma and its peripheral process – a relationship which thus far has been primarily discussed in the context of theoretical models (e.g., Javel and Shepherd, 2000; Rattay et al., 2001; Briaire and Frijns, 2006).

## 2. Methods

### 2.1. Animals and experimental design

The histological and functional data presented in this study were obtained from several previous studies and have partly been presented before (van Loon et al., 2013; Ramekers et al., 2014, 2015a; Kroon et al., 2017). For detailed descriptions of the methods regarding surgical treatment and electrophysiological procedures we refer to those studies below. In total thirty-nine female albino guinea pigs were included in this study (strain: Dunkin Hartley; supplier: Harlan Laboratories, Horst, the Netherlands). The animals were treated according to one of five experimental procedures, as shown in Fig. 1 and described below. All experimental procedures were approved by the Animal Care and Use Committee of Utrecht University (DEC-UMC 03.04.036; DEC 2010.I.08.103; before 2015) or by the Dutch Central Animal Experiments Committee (since 2015; CCD 11500201550).

Normal hearing (auditory brainstem response [ABR] threshold $\leq$40 dB SPL) was confirmed in all animals prior to any experimental procedure. A threshold elevation $\geq$50 dB after the ototoxic treatment was considered to indicate successful deafening. The acutely implanted normal-hearing (NH; N = 6), two-weeks deaf (2WD; N = 6), and six-weeks deaf (6WD; N = 6) animals were implanted with an intracochlear electrode array shortly before termination and histological processing (Ramekers et al., 2014). The acutely implanted fourteen-weeks deaf animals (14WD; N = 4) were treated similarly (Kroon et al., 2017). The chronically implanted NH (N = 6) and fourteen-weeks deaf (14WD; N = 6) animals were implanted with an intracochlear electrode array 12 weeks prior to eCAP recordings and subsequent termination (Ramekers et al., 2015a). By means of an osmotic pump, phosphate-buffered saline (PBS) was infused into the scala tympani of these animals for four weeks. This treatment served as a negative control treatment that did not lead to histological differences between the treated right and the untreated left ear (for details see Ramekers et al., 2015a). From all aforementioned animals eCAP recordings are presented in this study. Finally, the one-week deaf animals (1WD; N = 5) did not receive any kind of surgery other than the deafening treatment one week before termination (van Loon et al., 2013); eCAP recordings were therefore not available for these animals.

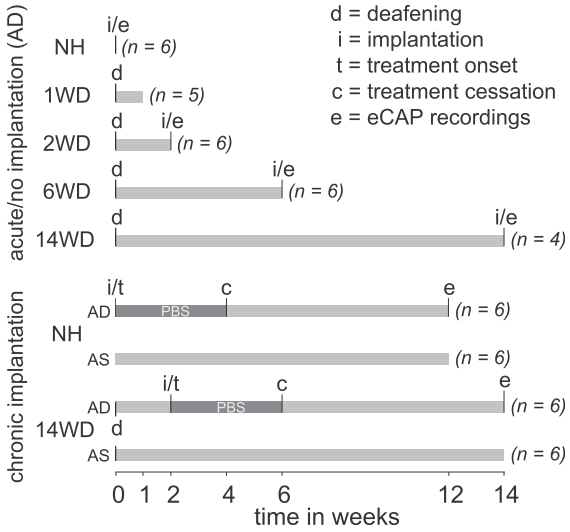


**Fig. 1.** Animal treatment schedule per experimental group. From five acutely implanted animal groups only the implanted right ears (auris dextra; AD) were used; from two additional groups of chronically implanted animals both the right implanted ears (AD) and the left (auris sinistra; AS) non-implanted ears were used. Chronic implantation was accompanied by four-week osmotic-pump-mediated infusion of phosphate-buffered saline (PBS) into the scala tympani as negative control treatment used in a previous study (Ramekers et al., 2015a). The end of the bars represent termination of the animals. All animals except for the 1WD group were subjected to eCAP recordings immediately prior to euthanasia and subsequent histological processing. The number of ears per group are given in brackets.

### 2.2. Deafening procedure

After induction of anesthesia (0.25 mg/kg dexmedetomidine and 40 mg/kg ketamine i.m.) click-evoked ABRs were recorded in order to confirm normal hearing. Deafening was executed by subcutaneous injection of kanamycin (Sigma-Aldrich, St. Louis, MO, USA; 400 mg/kg) and subsequent infusion of furosemide (Centrafarm, Etten-Leur, the Netherlands; 100 mg/kg) into the external jugular vein, which has been shown to eliminate the majority of both inner and outer hair cells (West et al., 1973; Versnel et al., 2007).

Histological evaluation of hair cell survival was performed in single midmodiolar sections in which for seven cross-sections of the organ of Corti hair cell presence can be determined (see Fig. 2A). Acoustic hearing was assessed with ABRs immediately prior to

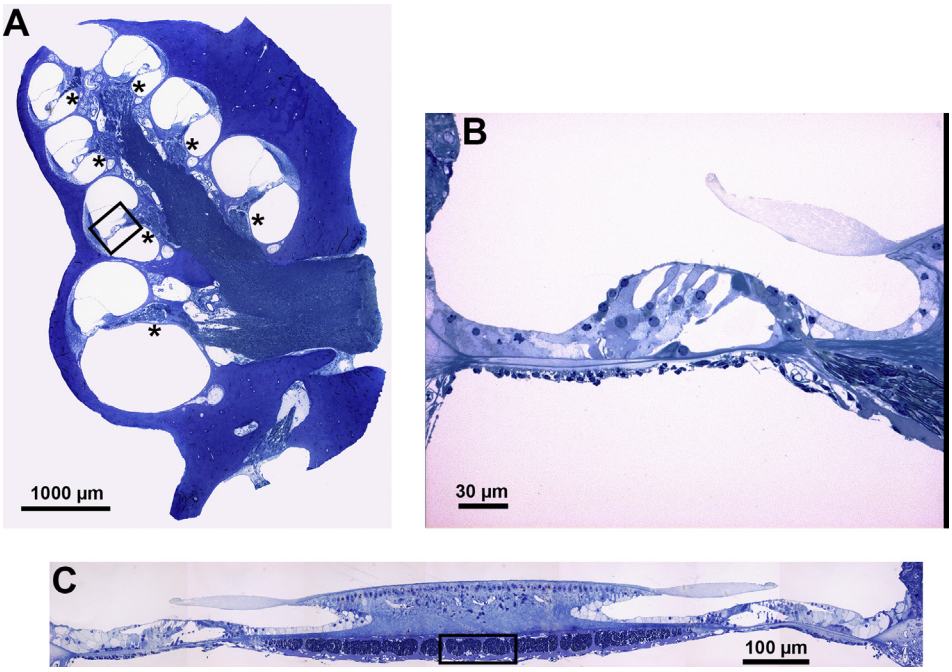


**Fig. 2.** **A** Midmodiolar cochlear section used for determination of SGC packing density in Rosenthal's canal (indicated by asterisks in the adjacent scala tympani). The black rectangle indicates the organ of Corti depicted in B. **B** Transection through the organ of Corti, including the osseous spiral lamina (OSL) through which the PPs protrude. The black line indicates the cutting plane through the OSL used for PP analysis, as shown in C. **C** Transection through the cochlea parallel to the midmodiolar section in A; on either side an obliquely sectioned organ of Corti is visible. Only the perpendicularly cut PPs in the center of this section (black rectangle) were analyzed.

termination and histological processing as previously described by Ramekers et al. (2014). In short, 20-µs clicks were presented to the right ear, starting at ~110 dB peak equivalent SPL and decreasing in 10-dB steps until the ABR had fully disappeared. The ABR threshold was subsequently defined as the interpolated sound level at which the ABR amplitude was 0.3 µV.

### 2.3. Cochlear implantation and eCAP recordings

The animals were anesthetized (0.25 mg/kg dexmedetomidine and 40 mg/kg ketamine i.m.) and their right bulla was exposed via a retro-auricular approach. The bulla was subsequently opened to expose the cochlea, in which a cochleostomy was drilled near the round window. Chronic implantation was done with a two-contact electrode array and a cannula connected to the subcutaneously positioned osmotic pump (Ramekers et al., 2015a). The electrode connector was fixed onto the skull with dental cement for eCAP recordings. Acute implantation was done with a four-contact electrode array (Ramekers et al., 2014). In both situations the most apical contact was used for stimulation and the most basal one for recording.

eCAP recordings were performed with a MED-EL PULSAR$_{CI}^{100}$ cochlear implant (MED-EL GmbH, Innsbruck, Austria), controlled by a PC via a Research Interface Box 2 (RIB2; Department of Ion Physics and Applied Physics, University of Innsbruck, Innsbruck, Austria) and a National Instruments data acquisition card (PCI-6533, National Instruments, Austin, TX, USA). Stimuli consisted of biphasic current pulses (typically 800 µA) with 30 µs phase duration and 30 µs inter-phase gap, which were presented with alternating polarity to reduce the stimulation artifact. The eCAP $N_1$ amplitude was defined as the voltage difference between $N_1$ and $P_2$. The $P_2$–$N_2$–$P_3$ complex was used to determine the amplitude of the secondary $N_2$ peak by first drawing a line from the $P_2$ to the $P_3$ peak; the $N_2$ amplitude then was defined as the shortest distance from this line (i.e., perpendicular) to the $N_2$ peak (see also: Ramekers et al., 2015b).

### 2.4. Histological analysis

For the acutely implanted animals only the right cochleas were used for the present study. Since long-term effects of chronic electrode presence in the cochlea might be expected, we included both the right implanted and the left non-implanted cochleas from the chronically implanted animals. Tissue fixation, histological processing, and analysis of SGC packing densities were largely performed as previously described by van Loon et al. (2013). In short, intra-labyrinthine cochlear fixation was achieved with a fixative of 3% glutaraldehyde, 2% formaldehyde, 1% acrolein and 2.5% DMSO in a 0.08 M sodium cacodylate buffer. The cochleas were then decalcified in 10% EDTA, secondarily fixed in 1% osmium tetroxide and 1% potassium ruthenium cyanide, and embedded in Spurr's low-viscosity resin. Staining was done with 1% methylene blue, 1% azur B, and 1% borax in distilled water.

Processing of the cochleas in order to obtain sections suitable for determination of the packing density of the SGC somata and PPs is described below. Note that throughout this report the SGC somata are simply referred to as "SGCs", while strictly this term includes their peripheral processes as well.

#### 2.4.1. Spiral ganglion cells

After dividing the cochleas into two halves along a standardized midmodiolar plane, they were re-embedded in fresh resin. From each cochlea five semi-thin (1-µm) sections (only three sections for the chronically implanted animals) were cut at 30-µm intervals (Fig. 2A). Using a 40 × oil immersion objective, micrographs of each transection of Rosenthal's canal were obtained (2 basal, 2 middle, and 3 apical transections for NH, 2WD, 6WD and 14WD animals; 2 basal and 2 middle transections for 1WD animals). The number of type-I and type-II SGCs was determined and the packing density was averaged across sections. It was subsequently averaged in

order to obtain one value per cochlear location (base, middle and apex); these averages were then averaged to obtain a single value per cochlea. Since the likelihood of detecting an individual SGC depends on its perikaryal size, the packing density was corrected for perikaryal size as previously described (Coggeshall and Lekan, 1996; van Loon et al., 2013).

#### 2.4.2. Peripheral processes

Processing and analysis with respect to PP packing densities have previously been described by Waaijer et al. (2013). Semi-thin sections were cut parallel to the midmodiolar plane at the level of the osseous spiral lamina (OSL) indicated by the black line in Fig. 2B, for the basal, middle, and apical turn separately. With this method the location of PP analysis for each of the three cochlear turns is roughly in between the two corresponding locations for SGC analysis (±90° from either); e.g., the basal site for PP analysis is 90° apical from the lower basal turn and 90° basal from the upper basal turn. Since we used the average of SGC packing densities at those two locations, which effectively is an estimate of SGC packing density at the location of PP analysis, we do not expect a systematic difference between SGC and PP counts. Micrographs were obtained using a 63 × oil immersion objective, yielding an approximately 110-μm wide transection of the OSL containing the PPs (Fig. 2C). Packing densities were determined by delineating the bony boundaries of the OSL and subsequently dividing the number of PPs by the thus obtained transectional area of the OSL. Note that evaluation of PPs at this level only allows for assessment of the myelinated portion of the PPs; the unmyelinated portion beyond the habenula perforata was not examined.

Ultrastructural qualitative analysis of PPs was done using transmission electron microscopy. An LKB Bromma 8800 Ultrotome III microtome (LKB Bromma, Sweden) was used to cut ultrathin (90–100 nm) sections of the OSL in a total of ten cochleas (from three NH, two 2WD, two 6WD and three 14WD animals; all of which acutely implanted). Sections were contrasted with 7% uranyl acetate in 70% methanol and Reynold's lead citrate (Reynolds, 1963) and examined using an FEI Tecnai 12 electron microscope (Field Electron and Ion Company, Hillsboro, OR, USA) at 80 kV. At 1500 × magnification micrographs were captured and merged off-line in order to be able to evaluate approximately the same ~110 μm as previously with light microscopy. This analysis was performed to evaluate the appearance of PPs in the degenerating situation in greater detail than possible with light microscopy, and encompassed assessment of damage to or disruption of the axoplasm or myelin sheath. If necessary higher magnification micrographs (6000×) were used, as exemplified in Fig. 4.

### 2.5. Data analysis and statistics

The time course of degeneration for SGCs and their PPs was determined by fitting of the data with an exponential function (following Versnel et al., 2007):

$$pd = e^{-\frac{t}{\tau}}, \qquad \text{(Eq. 1)}$$

where $pd$ is the packing density normalized to the average for NH animals, $t$ is time in weeks, and $\tau$ is the degeneration time constant.

Packing densities were subsequently normalized by dividing by the mean values for the six non-implanted NH ears (see section 3.3. for details); eCAP amplitudes were normalized by dividing by the mean values for all twelve implanted NH ears. Pearson's correlation coefficient was calculated to characterize the relation between PP and SGC packing densities, and between eCAP amplitudes and SGC or PP packing densities. Since the normalization causes all regression lines to go through point (1,1), a slope of 1 would mean a proportional decrease toward 0 for both variables; a slope steeper or shallower than 1 would imply that the decrease was disproportional – for instance faster degeneration of PPs than of SGCs.

All statistical analyses were performed using the Statistics Toolbox in MATLAB (version 7.11.0; Mathworks, Natick, MA, USA).

## 3. Results

### 3.1. Assessment of normal hearing and ototoxic deafening

Estimations of hair cell presence for most of the animals in the present study have been presented previously (van Loon et al., 2013; Ramekers et al., 2014, 2015a). All three NH groups had near-complete inner hair cell (IHC) and outer hair cell (OHC) presence (mean across animals for acutely implanted: 100% IHCs and 96% OHCs; for chronically implanted: 100% IHCs and 100% OHCs; for non-implanted: 100% IHCs and 98% OHCs). As we have observed previously (Ramekers et al., 2015a), with time after deafening the hair cells gradually disappeared (1WD: 72% IHCs and 32% OHCs; 2WD: 45% IHCs and 37% OHCs; 6WD: 13% IHCs and 18% OHCs; 14WD acutely implanted: 0% IHCs and 6% OHCs; 14WD chronically implanted: 2% IHCs and 5% OHCs; 14WD non-implanted: 0% IHCs and 8% OHCs).

All animals had normal hearing prior to any surgical intervention, as verified by click-evoked ABRs (Ramekers et al., 2014, 2015a): mean ABR threshold across all ears was 31 dB peak-equivalent SPL and did not differ among groups (one-way ANOVA; $F_{(7,44)} = 0.81$; $p = 0.59$). The chronically implanted NH animals on average had a threshold increase of only 10 dB twelve weeks after implantation (from 28 to 38 dB SPL). Since we did not observe hair cell loss in these animals, this shift was most probably related to the modified cochlear mechanics caused by the presence of the intracochlear electrode. The non-implanted and acutely implanted NH animals had mean ABR thresholds of 32 and 29 dB SPL, respectively. The mean threshold shift after deafening across all deafened groups was 72 dB (range 50–86 dB).

### 3.2. Examples of SGC degeneration

Examples of micrographs showing PPs and SGCs are depicted in Fig. 3 for one individual animal per time point after deafening. The loss of PPs and SGCs is discernible from two weeks after deafening onwards, but it becomes clearly visible six and fourteen weeks after deafening from the absence of tissue within the bony boundaries.

In Fig. 4 representative examples of electron micrographs are shown for a NH (A) and a 14WD animal (B). Again, the loss of processes in the 14WD animal is clearly visible, but the appearance of the surviving PPs is similar to that of the NH animal.

### 3.3. Quantification and comparison of packing densities

Differences in SGC packing density among the three NH conditions (acutely implanted, chronically implanted and non-implanted) were small (Fig. 5A). Since the electrode array was located in the basal turn, we performed one-way ANOVA on the results in this location only. Significant differences among groups were not observed ($F_{(2,15)} = 1.6$; $p = 0.23$). As with SGC packing densities, differences among the three groups in the NH condition for PP packing densities were non-significant (Fig. 5B; $F_{(2,15)} = 0.64$; $p = 0.54$).

The time course of degeneration for both the SGCs and PPs is shown in Fig. 6. Degeneration was found to be similar for SGCs ($\tau = 9.0$ weeks; Fig. 6A) and PPs ($\tau = 9.1$ weeks; Fig. 6B). In other words, 63% ($1\text{-}e^{-1}$) of SGCs was lost after 9 weeks, at which time PP degeneration had almost reached this same level. Accordingly,

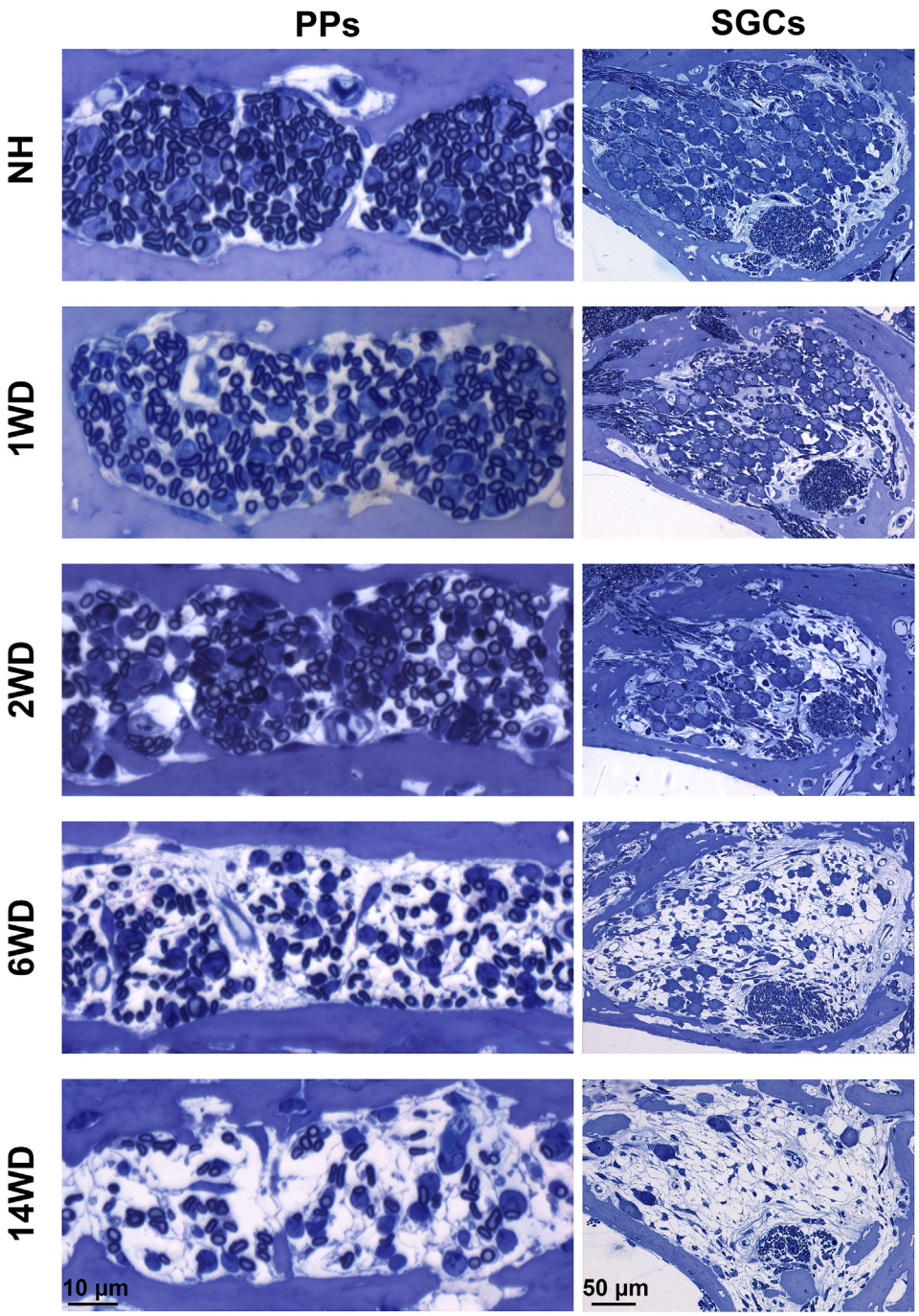


**Fig. 3.** Examples of histological sections for an NH (**A**, **B**), a 1WD (**C**, **D**), a 2WD (**E**, **F**), a 6WD (**G**, **H**), and a 14WD animal (**I**, **J**). The left column shows the OSL containing the PPs in the basal turn; the right column shows the SGCs in Rosenthal's canal in the upper basal turn. A gradual degeneration of both neural elements is clearly visible.

strong and highly significant correlations were observed between normalized PP and SGC packing densities for all three cochlear locations ($R^2 \geq 0.88$; $P < 0.001$; Fig. 7). More importantly, the slopes of the regression lines were close to 1 and the intercepts close to 0, indicating simultaneous onset as well as a similar rate of degeneration for SGCs and their PPs.

### 3.4. Cross-sectional area

In Fig. 8 the mean cross-sectional areas of both neural elements are presented. Across the three different NH conditions the SGC perikaryal area did not vary (Fig. 8A), suggesting that any form of electrode insertion trauma does not directly affect the cell soma. In contrast, their PPs appear to swell up considerably immediately but transiently upon implantation (compare acutely implanted with chronically implanted animals in Fig. 8B). Interestingly, this increase in fiber diameter compared to both chronically implanted and non-implanted cochleas reached far beyond the cochlear basal turn in which the electrode array resided (mean across all three locations – one-way ANOVA: $F_{(2,15)} = 5.6$; $P = 0.015$; post-hoc Bonferroni: acute versus chronic implantation: $P = 0.030$, acute implantation versus non-implanted: $P = 0.036$). Electron

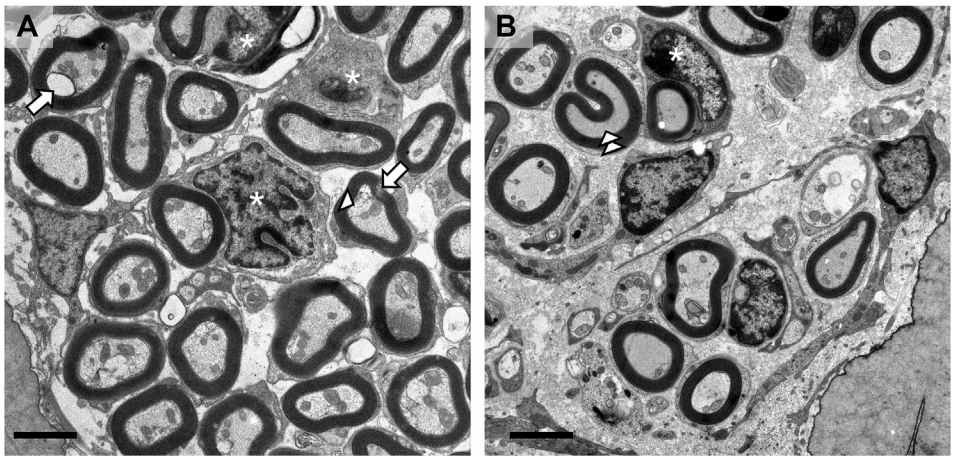


**Fig. 4.** Transmission electron microscopic image of the cochlear osseous spiral lamina of a NH animal (**A**) and of a 14WD animal (**B**). Whereas the PP packing density has clearly decreased after deafening, overall appearance of the processes and their myelin sheath is similar for the two conditions. Asterisks, Schwann cells; arrows, myelin disruption; arrow head, axoplasm disruption; double arrow head, flattened PP; scalebar: 2 μm; magnification 6000x.

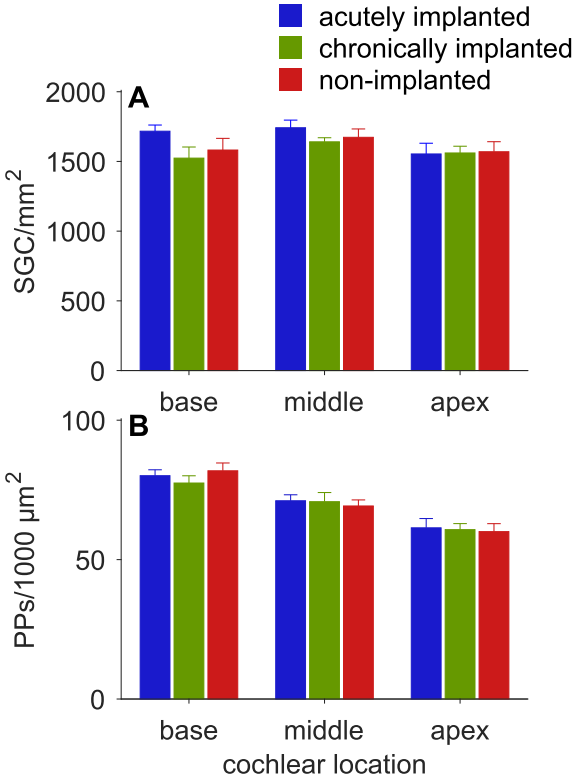


**Fig. 5.** Numerical packing densities of SCG somata (**A**) and their PPs (**B**) shown for three cochlear locations separately, and for three NH conditions: acutely implanted ears, chronically implanted ears, and non-implanted contralateral ears of the same chronically implanted animals. Differences among NH conditions are non-significant (see section 3.2). N = 6 for all groups; error bars represent SEM.

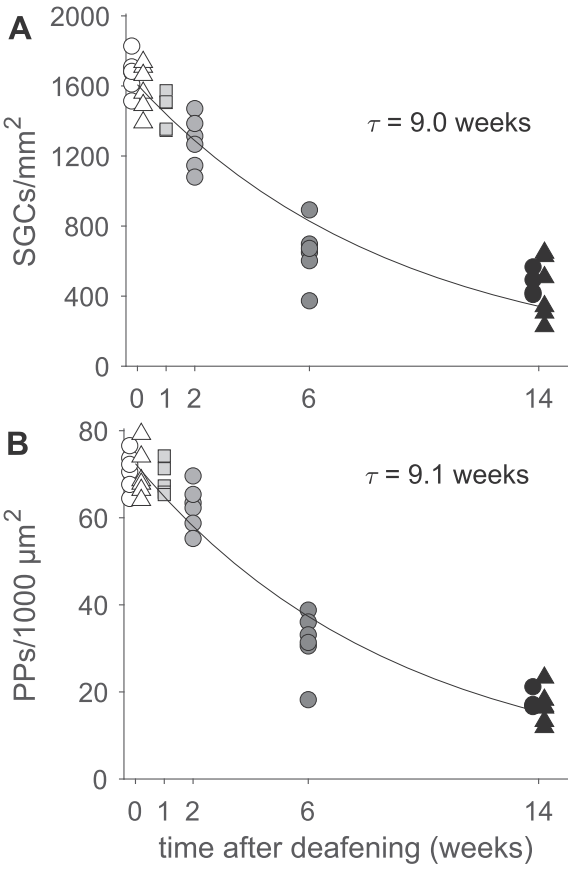


**Fig. 6.** Time course of degeneration of the SGC somata (**A**) and that of their PPs (**B**) after ototoxic treatment. Fitting of these data with Eq. (1) yielded a degeneration time constant $\tau$ that is similar for both neural elements. Circles represent acutely implanted animals (NH, 2WD, 6WD, 14WD); triangles represent chronically implanted animals (NH, 14WD); squares represent non-implanted animals (1WD).

microscopical analysis of these enlarged PPs did not show any apparent additional pathological features, as exemplified in Fig. 8D (chronically implanted NH) and Fig. 8E (acutely implanted NH).

Consistent with a wealth of previous reports, the mean SGC perikaryal area decreased after deafening (Fig. 8C). For the two time points available for chronically implanted cochleas, the mean PP cross-sectional axoplasm area follows the same course. The much more fluctuating PP size for acutely implanted cochleas suggests that even within the bony confinements of the OSL, these fibers are susceptible to electrode insertion into the scala tympani.

### 3.5. Ultrastructural appearance

In order to verify that the PPs quantified using light microscopy

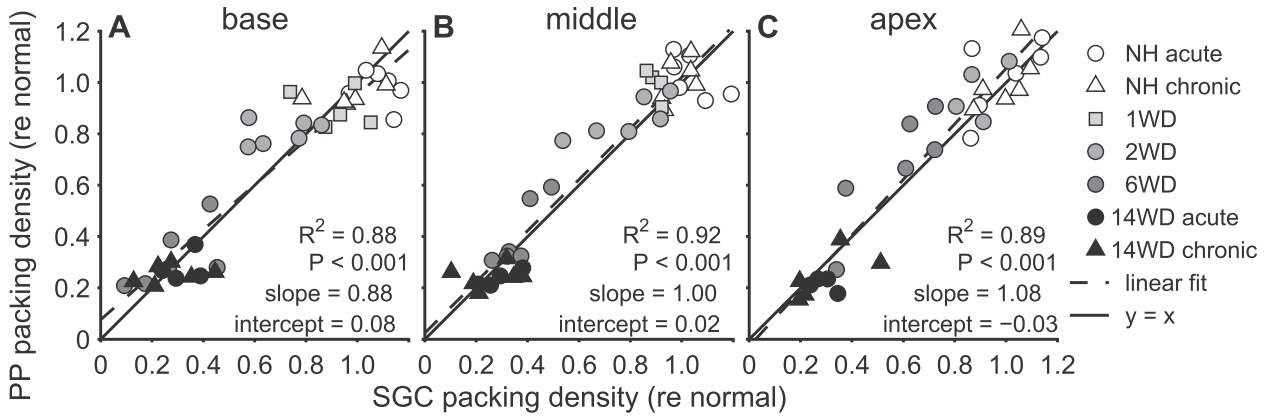


**Fig. 7.** Correlations between PP packing density and SGC packing density for the three cochlear locations: base (**A**), middle (**B**), and apex (**C**). Packing densities are normalized to the mean values of the non-implanted NH ears, for each location separately. Dashed lines are linear regression lines – $R^2$ and $P$ values for the corresponding correlations as well as slope and intercept of the regression line are shown in each plot. Solid lines are defined by $y = x$, and therefore visualize the relation between PPs and SGCs in case of simultaneous degeneration. The close resemblance between the two lines in all three plots strongly suggests simultaneous degeneration of the SGC soma and its PP.

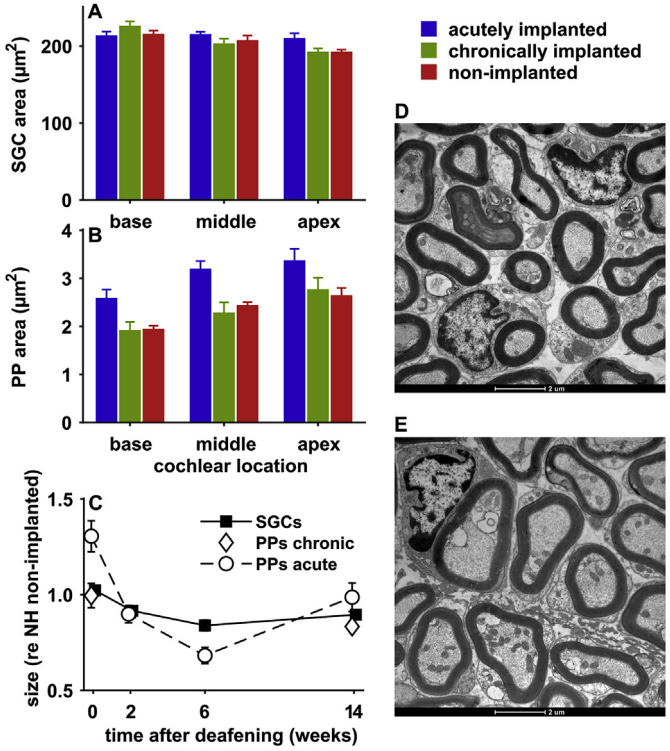


**Fig. 8.** Mean perikaryal area of SGCs (**A**) and mean PP axoplasm area (**B**) shown for three cochlear locations separately, and for three NH conditions: acutely implanted ears, chronically implanted ears, and non-implanted contralateral ears of the same chronically implanted animals. **C** Transectional area of both neural elements as function of time after deafening, normalized to the non-implanted (left) ears of NH animals. PP size is shown for acutely implanted and chronically implanted animals separately; mean SGC soma size is averaged across all three conditions (acutely, chronically and non-implanted). Error bars represent SEM. **D** SEM example of PPs in the middle cochlear turn of a chronically implanted NH animal. **E** SEM example of PPs in the middle cochlear turn of an acutely implanted NH animal, showing enlarged but seemingly healthy peripheral processes.

were in fact viable nerve fibers, we performed electron microscopy on a subset of the analyzed cochleas. In three NH, two 2WD, two 6WD and three 14WD cochleas (all acutely implanted) a total of 6603 structures were thus positively identified as being a well-myelinated PP. Neither in the NH controls nor in any of the deaf cochleas did we observe any empty myelin sheaths (as evidence for degenerated processes) or unmyelinated (or thinly myelinated) afferent processes. This finding confirms that PP quantification based on light microscopic images, with only a limited level of detail, is an adequate method.

The 6603 examined PPs were furthermore classified based on their appearance. The observed conditions were healthy and well-myelinated (NH: 94.2%; 2WD: 91.4%; 6WD: 90.6%; 14WD: 90.6%), overall healthy but with slight disruption of either the axoplasm or the myelin sheath (NH: 5.6%; 2WD: 6.8%; 6WD: 5.1%; 14WD: 8.9%), or considerably flattened (NH: 0.2%; 2WD: 1.9%; 6WD: 4.2; 14WD: 0.6%). The differences between groups are small, indicating that it is unlikely that PP counts may have been substantially biased by inclusion of degenerating fibers in one group or the other.

### 3.6. eCAP amplitude

Both the eCAP $N_1$ and $N_2$ amplitude decreased after deafening, as exemplified in Fig. 9A. The mean eCAP amplitude for all 12 implanted NH animals was 1.6 mV and 0.10 mV for $N_1$ and $N_2$ peaks, respectively, and these values were used to normalize all eCAP amplitudes for further analysis. Since the amplitude of both peaks decreased after deafening, there was an obvious correlation between the two across all animals (Fig. 9B), although almost 80% variance remained unexplained; i.e., the decrease in $N_1$ amplitude after deafening was not accompanied by a proportional decrease in $N_2$ amplitude. We therefore sought to identify an anatomical measure that could explain the differential effects of deafness on both peaks' amplitudes.

Consistent with our hypothesis that having relatively many PPs produces a larger $N_2$ peak, on the one hand the $N_1$ amplitude correlated well with SGC packing density (Fig. 10A), and on the other hand the $N_2$ amplitude correlated equally well with PP packing density (Fig. 10B). However, for the hypothesis to be completely accurate, in addition the relative number of PPs over SGCs should correlate with the $N_2/N_1$ amplitude ratio, since having relatively many PPs should result in a relatively large $N_2$ peak. In contrast, Fig. 10C suggests that the large variability in the relative eCAP $N_2$ peak amplitude cannot be explained by the considerably more consistent peak ratio across animals. Moreover, the table in Fig. 10D reveals that the four possible correlations between eCAP peaks and packing densities are strikingly similar, indicating that based on these data it is not possible to link any one functional measure to one of the two histological measures.

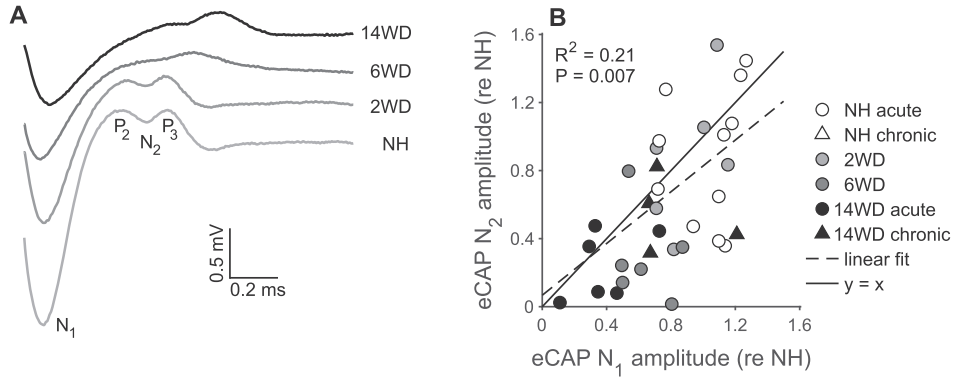


**Fig. 9.** **A** Examples of eCAP recordings in response to a 50-μs 480-μA biphasic stimulus for four individual animals. The voltage difference between the $N_1$ and $P_2$ peaks defines the eCAP $N_1$ amplitude; the $P_2$–$N_2$–$P_3$ peak complex defines the $N_2$ amplitude (see text for definition). **B** Relation between the $N_2$ and $N_1$ amplitude, both normalized to the respective mean implanted NH values. The correlation is statistically significant but remarkably weak.

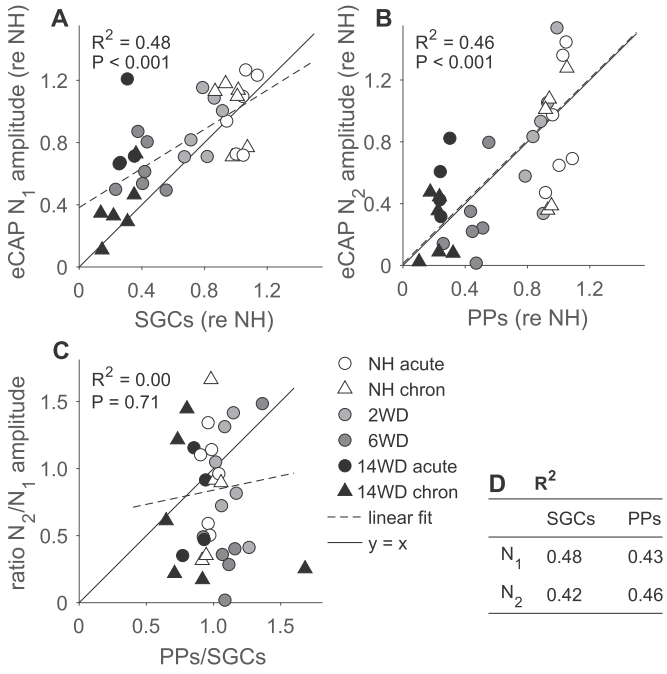


D $R^2$

| | SGCs | PPs |
|---|---|---|
| $N_1$ | 0.48 | 0.43 |
| $N_2$ | 0.42 | 0.46 |

**Fig. 10.** **A** eCAP $N_1$ amplitude plotted as function of across-cochlear averages of SGC packing density. **B** eCAP $N_2$ amplitude plotted as function of across-cochlear averages of PP packing density. All packing densities and eCAP amplitudes shown are normalized to the respective mean values for implanted NH ears. **C** The ratio of $N_2$ over $N_1$ amplitude plotted as function of the ratio of PP over SGC packing density. Dashed lines are regression lines – $R^2$ and $P$ values for the correlations are shown in each plot; solid lines represent $y = x$. **D** The $R^2$ for all four possible correlations between eCAP amplitude and neural packing densities. The correlations as shown in **A** and **B** yield the highest proportion of explained variance, but the differences are small.

## 4. Discussion

In a retrospective experimental design we have analyzed in detail the degeneration of SGCs and that of their peripheral processes in thirty-three cochleas at various time points after deafening, and compared it to the healthy condition in eighteen additional cochleas. In accordance with a wealth of literature, both neural elements degenerated substantially over a time course of several weeks: gradual loss was accompanied by shrinkage of the remaining structures. Notably, both the onset and the rate of degeneration were highly similar for the two elements of the SGC, indicating there was no gradual retrograde degeneration. Furthermore, the subtle variability that did exist between the two courses of degeneration clearly did not predict the relative amplitude of the eCAP $N_2$ peak. This absence of any relation suggests that the two peaks in the eCAP waveform cannot be attributed to the existence of two distinct sites of excitation – one central and one peripheral to the SGC soma.

### 4.1. Simultaneous degeneration

It was expected that the SGCs would either degenerate at a slower or at a similar rate compared to their PPs, based on the fact that neurites normally die within 1–2 days after the connection with the soma is lost (Mack et al., 2001). The regression lines resulting from the correlation between PP and SGC packing density approximated $y = x$ (Fig. 7), which strongly implies that degeneration of an SGC and its PP occurred simultaneously. The degeneration time course was slightly faster for PPs than for their cell bodies (Fig. 6), which may well be within the margins of error. Alternatively, since the packing density of SGCs was averaged across two transections of Rosenthal's canal per location (being base, middle and apex), and the PP packing density was sampled in the OSL in between these two (i.e., at a 90° angle from either transection), local fluctuations in survival possibly confound the data to a certain extent.

### 4.2. Simultaneous versus retrograde degeneration

The present findings do not support the idea that degeneration of SGCs after hair cell loss proceeds in a gradual retrograde fashion, since a clear simultaneous loss of SGCs and PPs was observed. This finding contrasts with several previous findings. In deafened cats PPs have been reported to degenerate prior to SGC loss (Liberman and Kiang, 1978; Spoendlin, 1984; Leake and Hradek, 1988; Xu et al., 1993; Shepherd and Javel, 1997). However, some of these concern case reports, or do not provide quantification, and differences in survival rate between SGCs and PPs frequently lack statistical corroboration. In a quantitative study in deafened chinchillas, McFadden et al. (2004) found a gradual decrease in SGC packing density similar to that in the present study, but PPs had almost completely degenerated as soon as two weeks after deafening indicating retrograde degeneration. Given that the means of deafening varied widely among (and occasionally within) the aforementioned studies (noise exposure, intramuscular injections of neomycin, single co-administration of kanamycin and ethacrynic acid, repeated administration of kanamycin, intracochlear direct current stimulation, or co-administration of gentamycin and

ethacrynic acid), it is tempting to classify the difference between the present findings and theirs as being species-related rather than being dependent on the cause of deafness.

In a recent study in guinea pigs Wise et al. (2017) concluded that degeneration of PPs preceded that of their cell bodies in an experimental set-up remarkably similar to ours. However, their conclusion was not based on direct comparison of the two neural elements. Rather, they reported statistically significant PP degeneration (i.e., decrease in fiber diameter) in 2WD animals, while any significant effect on SGC somata was only observed in 6WD animals (i.e., decrease in SGC packing density). Nevertheless, when analyzed identical to our data presented here, their data both from the aforementioned study as well as from their previous study on PP degeneration (Wise et al., 2005) is highly similar to ours: seemingly simultaneous degeneration of PPs and their cell bodies. As these findings are therefore in accordance with the present study, they add to the likelihood of a species-related difference in the degeneration process of SGCs after deafening.

It is generally believed that SGC degeneration in humans follows a retrograde course, but evidence for this is not unambiguous. Histopathological studies mainly present case reports and often do not quantify presence of PPs (e.g., Otte et al., 1978; Hinojosa and Marion, 1983; Hinojosa et al., 1987; Nadol et al., 1989; Lu and Schuknecht, 1994). While Hinojosa and Marion (1983) reported severe loss of PPs in four patients with SGC presence of up to 50%, this was not the case for all patients, and one even appeared to have more PPs than SGCs. Moreover, based on detailed counts in cochleas from deaf patients and normal-hearing controls, Spoendlin and Schrott (1989) concluded that a PP only disappears when the SGC degenerates. These reports based on histological quantifications are in line with the simultaneous degeneration reported in the present study.

### 4.3. PP size and ultrastructural appearance

Shrinkage of the SGC somata and their PPs following ototoxic deafening has been frequently reported before (e.g., Wise et al., 2005, 2017; Agterberg et al., 2008; Glueckert et al., 2008; Waaijer et al., 2013). Decrease of the mean cell size or fiber diameter may reflect either ongoing degeneration of part of the population, or a (possibly reversible) process associated with functional redundancy due to hair cell loss. As we have argued previously, since we do not observe a division in the distribution of SGC cross-sectional area between normal-sized healthy and shrunken degenerating cells (van Loon et al., 2013), the latter explanation is more appealing. On the other hand, increases in mean size between six and fourteen weeks after deafening (Fig. 8C) arguably reflects the loss of all SGCs/PPs that had initially shrunken while only few normal-sized healthy cells remain. The present electron microscopic analysis and the light microscopic examples in Fig. 3 – as well as histological examples from Waaijer et al. (2013) and Wise et al. (2017) – may serve as evidence for this alternative explanation: somewhat flattened PPs appear to be more common in 6–8 weeks deaf guinea pigs than in 14WD animals.

In stark contrast to the findings of Wise et al. (2017), we did not observe any myelin sheaths completely devoid of PPs in the electron microscopic analysis of both NH and deafened cochleas. In fact, we observed only minor disruptions of either axoplasm or myelin in all four examined groups, suggesting that these observations might reflect fixation artifacts rather than ongoing degeneration. We do not have a satisfying explanation for the absence of empty myelin sheaths in our preparations, given that these have been reported previously in both guinea pigs (Wise et al., 2017) and cats (Leake and Hradek, 1988) after aminoglycoside deafening.

Importantly, this detailed assessment of several thousand PPs convincingly indicated that – at least in the present data set – quantification of myelin using light microscopy suffices for reliable identification of PPs.

### 4.4. eCAP amplitude as a predictor for SGC survival

The eCAP $N_1$ amplitude correlated fairly well with SGC packing density (Fig. 10A). This finding is in agreement with previously reported correlations between the eABR $P_1$ peak amplitude and SGC counts (Hall, 1990) and between slope of the eCAP growth-function and SGC packing density (Pfingst et al., 2017). However, the eCAP $N_1$ amplitude correlated equally well with PP packing density, so that these data cannot be used to determine the site of action potential initiation, which may be at or near the SGC soma, or at its PP. Alternatively, if the eCAP $N_2$ peak amplitude had correlated better with PP packing density than the $N_1$ peak did, it would suggest that the $N_1$ peak is a result of excitation near the soma and the $N_2$ peak would have a more peripheral site of excitation. The data, however, do not support this theory, as both peaks correlated equally well with both packing densities (Fig. 10D). Likewise, the theory that there is one site of excitation (central) and the $N_2$ peak reflects antidromic action potentials into the PPs (e.g., Briaire and Frijns, 2005) is not supported by the present findings either, since the relative $N_2$ amplitude should even so correlate with relative PP presence. A possible explanation for the two peaks – one which is not contradicted by the present findings – is that there is a single site of excitation (e.g., at the SGC soma, and action potential initiation peripheral to the soma is not possible) and the secondary peak is repeated firing of (part of) the same population (as argued previously by Ramekers et al., (2015b) and Strahl et al., (2016)).

An interesting observation is that for both SGCs (Fig. 10A) and PPs (data not shown) the eCAP $N_1$ amplitude is higher at low packing densities than would be expected based on a linear relation, which is often assumed in CAP convolution models (e.g., Earl and Chertoff, 2010). The deviation from this assumption at low packing densities may reflect one of two mechanisms. First, it is possible that the remaining SGCs are stimulated more uniformly, as the population becomes smaller. Their responses may therefore be more synchronized, which results in a narrower eCAP with consequently larger amplitude. Second, demyelination of the remaining SGCs (Agterberg et al., 2008) or PPs (Wise et al., 2017) may lead to a larger amplitude for action potentials of individual SGCs as measured extracellularly.

### 4.5. Functional implications

The presence of PPs is believed to be beneficial for cochlear implant stimulation, since their closer proximity to the electrode array may lead to lower thresholds and improved tonotopic specificity (argued by e.g., Wise et al., 2005; Waaijer et al., 2013; Senn et al., 2017). It would therefore be important to preserve PPs in cochlear implant users. In numerous animal studies SGCs are shown to be successfully protected from degeneration by treatment with neurotrophic factors (for a review, see Ramekers et al., 2012), and several studies have shown that this protection includes that of PPs (Wise et al., 2005; Glueckert et al., 2008; Waaijer et al., 2013).

Apart from protection from degeneration, neurotrophic treatment has also been suggested as a means to induce regrowth of PPs toward the electrode array (e.g., Senn et al., 2017). Firstly, it should be investigated whether these fibers are actually electrically excitable – and, if so, whether this includes the non-myelinated portion protruding beyond the bony modiolar structures. Moreover, complete PP regrowth is obviously only of interest in case of slow retrograde degeneration, when SGCs are still abundant but

their PPs have already degenerated. As the present findings show, this type of degeneration may not be as self-evident as it is often claimed.

## Declaration of competing interest

None.

## Acknowledgments

The authors would like to thank Ferry Hendriksen for histological processing and EM analysis. This work was supported by MED-EL GmbH, Innsbruck, Austria.

## References

Agterberg, M.J.H., Versnel, H., De Groot, J.C.M.J., Smoorenburg, G.F., Albers, F.W.J., Klis, S.F.L., 2008. Morphological changes in spiral ganglion cells after intracochlear application of brain-derived neurotrophic factor in deafened Guinea pigs. Hear. Res. 244, 25–34.

Briaire, J.J., Frijns, J.H.M., 2005. Unraveling the electrically evoked compound action potential. Hear. Res. 205, 143–156.

Briaire, J.J., Frijns, J.H.M., 2006. The consequences of neural degeneration regarding optimal cochlear implant position in scala tympani: a model approach. Hear. Res. 214, 17–27.

Coggeshall, R.E., Lekan, H.A., 1996. Methods for determining numbers of cells and synapses: a case for more uniform standards of review. J. Comp. Neurol. 364, 6–15.

Earl, B.R., Chertoff, M.E., 2010. Predicting auditory nerve survival using the compound action potential. Ear Hear. 31, 7–21.

Glueckert, R., Bitsche, M., Miller, J.M., Zhu, Y., Prieskorn, D.M., Altschuler, R.A., Schrott-Fischer, A., 2008. Deafferentation-associated changes in afferent and efferent processes in the Guinea pig cochlea and afferent regeneration with chronic intrascalar brain-derived neurotrophic factor and acidic fibroblast growth factor. J. Comp. Neurol. 507, 1602–1621.

Hall, R.D., 1990. Estimation of surviving spiral ganglion cells in the deaf rat using the electrically evoked auditory brainstem response. Hear. Res. 49, 155–168.

Hinojosa, R., Marion, M., 1983. Histopathology of profound sensorineural deafness. Ann. N. Y. Acad. Sci. 405, 459–484.

Hinojosa, R., Blough, R.R., Mhoon, E.E., 1987. Profound sensorineural deafness: a histopathological study. Ann. Otol. Rhinol. Laryngol. 96 (Suppl. 128), 43–46.

Javel, E., Shepherd, R.K., 2000. Electrical stimulation of the auditory nerve. III. Response initiation sites and temporal fine structure. Hear. Res. 140, 45–76.

Kroon, S., Ramekers, D., Smeets, E.M., Hendriksen, F.G.J., Klis, S.F.L., Versnel, H., 2017. Degeneration of auditory nerve fibers in Guinea pigs with severe sensorineural hearing loss. Hear. Res. 345, 79–87.

Leake, P.A., Hradek, G.T., 1988. Cochlear pathology of long term neomycin induced deafness in cats. Hear. Res. 33, 11–33.

Liberman, M.C., Kiang, N.Y., 1978. Acoustic trauma in cats. Cochlear pathology and auditory-nerve activity. Acta Otolaryngol. 358, 1–63. Suppl.

Lu, C.B., Schuknecht, H.F., 1994. Pathology of prelingual profound deafness: magnitude of labyrinthitis fibro-ossificans. Am. J. Otol. 15, 74–85.

Mack, T.G.A., Reiner, M., Beirowski, B., Mi, W., Emanuelli, M., Wagner, D., Thomson, D., Gillingwater, T., Court, F., Conforti, L., Fernando, F.S., Tarlton, A., Andressen, C., Addicks, K., Magni, G., Ribchester, R.R., Perry, V.H., Coleman, M.P., 2001. Wallerian degeneration of injured axons and synapses is delayed by a Ube4b/Nmnat chimeric gene. Nat. Neurosci. 4, 1199–1206.

McFadden, S.L., Ding, D., Jiang, H., Salvi, R.J., 2004. Time course of efferent fiber and spiral ganglion cell degeneration following complete hair cell loss in the chinchilla. Brain Res. 997, 40–51.

Nadol Jr., J.B., 1990. Degeneration of cochlear neurons as seen in the spiral ganglion of man. Hear. Res. 49, 141–154.

Nadol Jr., J.B., Young, Y.S., Glynn, R.J., 1989. Survival of spiral ganglion cells in profound sensorineural hearing loss: implications for cochlear implantation. Ann. Otol. Rhinol. Laryngol. 98, 411–416.

Otte, J., Schuknecht, H.F., Kerr, A.G., 1978. Ganglion cell populations in normal and pathological human cochleae. Implications for cochlear implantation. Laryngoscope 88, 1231–1246.

Pfingst, B.E., Colesa, D.J., Swiderski, D.L., Hughes, A.P., Strahl, S.B., Sinan, M., Raphael, Y., 2017. Neurotrophin gene therapy in deafened ears with cochlear implants: long-term effects on nerve survival and functional measures. J. Assoc. Res. Otolaryngol. 18, 731–750.

Ramekers, D., Versnel, H., Grolman, W., Klis, S.F.L., 2012. Neurotrophins and their role in the cochlea. Hear. Res. 288, 19–33.

Ramekers, D., Versnel, H., Strahl, S.B., Smeets, E.M., Klis, S.F.L., Grolman, W., 2014. Auditory-nerve responses to varied inter-phase gap and phase duration of the electric pulse stimulus as predictors for neuronal degeneration. J. Assoc. Res. Otolaryngol. 15, 187–202.

Ramekers, D., Versnel, H., Strahl, S.B., Klis, S.F.L., Grolman, W., 2015a. Temporary neurotrophin treatment prevents deafness-induced auditory nerve degeneration and preserves function. J. Neurosci. 35, 12331–12345.

Ramekers, D., Versnel, H., Strahl, S.B., Klis, S.F.L., Grolman, W., 2015b. Recovery characteristics of the electrically stimulated auditory nerve in deafened Guinea pigs: relation to neuronal status. Hear. Res. 321, 12–24.

Rattay, F., Lutter, P., Felix, H., 2001. A model of the electrically excited human cochlear neuron. I. Contribution of neural substructures to the generation and propagation of spikes. Hear. Res. 153, 43–63.

Reynolds, E.S., 1963. The use of lead citrate at high pH as an electron-opaque stain in electron microscopy. J. Cell Biol. 17, 208–212.

Senn, P., Roccio, M., Hahnewald, S., Frick, C., Kwiatkowska, M., Ishikawa, M., Bako, P., Li, H., Edin, F., Liu, W., Rask-Andersen, H., Pyykkö, I., Zou, J., Mannerström, M., Keppner, H., Homsy, A., Laux, E., Llera, M., Lellouche, J.P., Ostrovsky, S., Banin, E., Gedanken, A., Perkas, N., Wank, U., Wiesmüller, K.H., Mistrík, P., Benav, H., Garnham, C., Jolly, C., Gander, F., Ulrich, P., Müller, M., Löwenheim, H., 2017. NANOCI-nanotechnology based cochlear implant with gapless Interface to auditory neurons. Otol. Neurotol. 38, e224–e231.

Shepherd, R.K., Javel, E., 1997. Electrical stimulation of the auditory nerve. I. Correlation of physiological responses with cochlear status. Hear. Res. 108, 112–144.

Spoendlin, H., 1975. Retrograde degeneration of the cochlear nerve. Acta Otolaryngol. 79, 266–275.

Spoendlin, H., 1984. Factors inducing retrograde degeneration of the cochlear nerve. Ann. Otol. Rhinol. Laryngol. 93 (Suppl. 112), 76–82.

Spoendlin, H., Schrott, A., 1989. Analysis of the human auditory nerve. Hear. Res. 43, 25–38.

Strahl, S.B., Ramekers, D., Nagelkerke, M.M.B., Schwarz, K.E., Spitzer, P., Klis, S.F.L., Grolman, W., Versnel, H., 2016. Assessing the firing properties of the electrically stimulated auditory nerve using a convolution model. Adv. Exp. Med. Biol. 894, 143–153.

van Loon, M.C., Ramekers, D., Agterberg, M.J.H., de Groot, J.C.M.J., Grolman, W., Klis, S.F.L., Versnel, H., 2013. Spiral ganglion cell morphology in Guinea pigs after deafening and neurotrophic treatment. Hear. Res. 298, 17–26.

Versnel, H., Agterberg, M.J.H., De Groot, J.C.M.J., Smoorenburg, G.F., Klis, S.F.L., 2007. Time course of cochlear electrophysiology and morphology after combined administration of kanamycin and furosemide. Hear. Res. 231, 1–12.

Waaijer, L., Klis, S.F.L., Ramekers, D., Van Deurzen, M.H.W., Hendriksen, F.G.J., Grolman, W., 2013. The peripheral processes of spiral ganglion cells after intracochlear application of brain-derived neurotrophic factor in deafened Guinea pigs. Otol. Neurotol. 34, 570–578.

Webster, M., Webster, D.B., 1981. Spiral ganglion neuron loss following organ of Corti loss: a quantitative study. Brain Res. 212, 17–30.

West, B.A., Brummett, R.E., Himes, D.L., 1973. Interaction of kanamycin and ethacrynic acid. Severe cochlear damage in Guinea pigs. Arch. Otolaryngol. 98, 32–37.

Wise, A.K., Richardson, R., Hardman, J., Clark, G., O'leary, S., 2005. Resprouting and survival of Guinea pig cochlear neurons in response to the administration of the neurotrophins brain-derived neurotrophic factor and neurotrophin-3. J. Comp. Neurol. 487, 147–165.

Wise, A.K., Pujol, R., Landry, T.G., Fallon, J.B., Shepherd, R.K., 2017. Structural and ultrastructural changes to type I spiral ganglion neurons and Schwann cells in the deafened Guinea pig cochlea. J. Assoc. Res. Otolaryngol. 18, 751–769.

Xu, S.A., Shepherd, R.K., Chen, Y., Clark, G.M., 1993. Profound hearing loss in the cat following the single co-administration of kanamycin and ethacrynic acid. Hear. Res. 70, 205–215.

Ylikoski, J., Wersall, J., Bjorkroth, B., 1974. Degeneration of neural elements in the cochlea of the Guinea pig after damage to the organ of corti by ototoxic antibiotics. Acta Otolaryngol. 326, 23–41. Suppl.

Zilberstein, Y., Liberman, M.C., Corfas, G., 2012. Inner hair cells are not required for survival of spiral ganglion neurons in the adult cochlea. J. Neurosci. 32, 405–410.